Available online at www.sciencedirect.com

SciVerse ScienceDirect

Procedia Environmental Sciences 18 (2013) 638 – 648

Procedia Environmental Sciences

2013 International Symposium on Environmental Science and Technology (2013 ISEST)

Microscopic and macroscopic properties of soils used as means for the interpretation of the efficiency of soil remediation technologies

Christos D. Tsakiroglou[a,*] , Christos A. Aggelopoulos[a,b]

[a]*Foundation for Research and Technology Hellas – Institute of Chemical Engineering Sciences, Stadiou str., Platani, 26504 Patras-Rio, Greece*

[b]*Laboratoire de Génie des Procédés Plasmas et Traitements de Surfaces - EA 3492, Université Pierre et Marie Curie - Ecole Nationale Supérieure de Chimie de Paris, Pierre & Marie Curie str., 75231 Paris Cedex, France*

Abstract

Reliable information for the multiphase transport coefficients of porous media (e.g. capillary pressure curve, relative permeability functions, hydrodynamic dispersion coefficients) is a prerequisite when investigating soil contamination and remediation processes. The majority of mineral soils are heterogeneous at multiple-scales but such characteristics are usually overlooked when measuring the effective transport coefficients. Transient immiscible and miscible displacement tests performed on long soil columns are coupled with inverse modeling algorithms to estimate the multiphase transport coefficients. Multipoint measurements of the electrical resistance are employed to determine the axial distribution of the fluid saturation as well as the solute concentration breakthrough curves. The transient responses of the solute concentration (breakthrough curve) over three cross-sections are inverted by using the one-region and two-region models so that the longitudinal dispersivity is estimated along with parameters quantifying the micro-heterogeneity at the pore network scale. The transient responses of the total pressure drop across the soil column, and fluid saturation averaged over five successive segments are inverted by using the single-permeability and multi-flow path model so that the dynamic capillary pressure and oil/water relative permeability curves are estimated along with parameters quantifying the macro-heterogeneity (e.g. permeability distribution) at the soil column scale. The measured multiphase transport properties are interpreted in terms of pore-scale parameters, and might be used for the interpretation of the efficiency of soil remediation technologies. The methodology is demonstrated with application to one homogeneous and one moderately heterogeneous soil used to test the non-thermal plasma discharge as a potential ex-situ remediation technology for mixtures of hydrocarbons.

Keywords: porous media; multiphase transport; relative permeability; capillary pressure; hydrodynamic dispersion; pore structure; soil heterogeneity; inverse modeling; soil remediation

* Corresponding author. Tel.: +30-2610-965212; fax: +30-2610-965223.
E-mail address: ctsakir@iceht.forth.gr.

doi:10.1016/j.proenv.2013.04.088

1. Introduction

The capillary pressure and relative permeability curves may be determined by performing either steady-state experiments with the simultaneous flow of both fluids through the porous medium [1] or transient experiments of the displacement of the one fluid by the other [2]. Albeit accurate, the steady-state methods are expensive and time-consuming. The transient experiments are fast and the two-phase flow coefficients are estimated implicitly by using the macroscopic two-phase flow equations, with history matching of the transient evolution of the pressure drop and spatial distribution of the fluid saturation [3,4]. The hydrodynamic dispersion coefficients are commonly estimated from datasets of miscible displacement experiments by fitting analytic or numerical solutions of the advection-dispersion equation to the transient variation of the solute concentration [4,5].

In the present work, immiscible and miscible displacement experiments are performed on fixed-bed columns of two soil types, and the electrical resistances measured between vertical ring electrodes and horizontal rod electrodes are converted to transient responses of water saturation and solute concentration, respectively. Numerical codes of inverse modeling of the two-phase flow and advection-dispersion equations are employed to estimate the capillary pressure curve, the relative permeability curves, and the longitudinal dispersion coefficient. The results are interpreted with reference to the pore structure of soils, and may be helpful in explaining the efficiency of soil remediation technologies.

2. Materials and methods

2.1. Experimental setup

The experimental apparatus for conducting miscible and immiscible displacement experiments on undisturbed soil columns (Fig.1a,b) has been described in detail in earlier work [6-8]. During the flow tests, the electrical conductance of the aqueous phase (NaCl solution) is monitored over various cross-sections and across successive segments of the soil column, and is converted to solute concentration and water saturation values, respectively [6-8].

Table 1. Properties of soils.

Soil	S1	S5
Grain size distribution	Narrow (125-200μm)	Broad* (<2μm-2mm)
Porosity, φ	0.4	0.45
Permeability, k	25×10^{-12} m^2	385×10^{-15} m^2
Formation factor, F	3.5	4.7

* d_g>125 μm: 69%; 50 μm<d_g<125 μm: 14%; 2 μm<d_g<50 μm: 4%; d_g<2 μm: 13%

Miscible displacement experiments were performed for two soil types differing with respect to the degree of micro-heterogeneity: soil S1 is a homogeneous silicate sand with narrow grain size distribution, and soil S5 is a loamy sand with a broad grain size distribution (Table 1). During miscible displacement tests (hydrodynamic dispersion experiments) a low NaCl concentration solution was displaced by a high NaCl concentration solution upwards and the electrical conductance over three cross-sections was measured by using three pairs of rod electrodes (Fig.1a). The transient response of the solute concentration (breakthrough curve) at each cross-section was determined by transforming the electrical conductivity values to solute concentration [9]. The characteristics of the breakthrough curves (solute

arrival times, tailing, and degree of overlapping) and the injected solution volume required before detecting NaCl molecules at the outlet (breakthrough time) are indicative of the type and degree of pore space heterogeneity [6,9].

During immiscible displacement drainage experiments, a wetting fluid (an aqueous solution of NaCl) was displaced by a non-wetting one (n-dodecane) downwards under a constant flow rate. Details about the experimental method are reported elsewhere [7]. During each test, the total pressure drop across the soil column, the effluent weight and the electrical resistance across five segments of the column were monitored. The electrical resistance was transformed to water saturation by using a non-Archie equation [10].

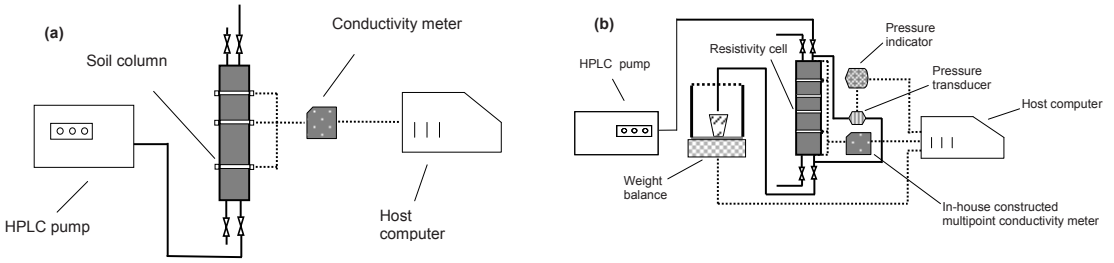

Fig. 1. Experimental setup for (a) miscible and (b) immiscible displacement experiments in soil columns.

2.2. Numerical modeling of miscible displacement

In a macroscopically homogeneous porous medium, the microscopic disorder may cause local perturbations of permeability (local heterogeneities), the intensity of which depends on the variability of the pore size distribution. In general, the transport of a conservative solute in a rigid porous medium is described by the advection-dispersion equation

$$\frac{\partial C}{\partial t} + \nabla \cdot \left(\mathbf{u}_p \, C \right) = \nabla \cdot \left(\mathbf{D} \cdot \nabla C \right) \qquad (1)$$

where $\mathbf{u}_p$ is the local pore velocity vector, and $\mathbf{D}$ is the local dispersion coefficient tensor. For one-dimensional flow the longitudinal dispersion coefficient is given by

$$D_L = D_{eff} + a_L u_p \qquad (2)$$

In a miscible displacement experiment, initially (t<0) the porous medium is fully saturated by a solution of low solute concentration, C_i , and at time t=0, a solution of high solute concentration, C_0 , is injected through the inlet port at a constant flow rate. If any local perturbations of the permeability are neglected, and the porous medium is regarded as homogeneous (Fig.2a), then the flow is one-dimensional, the pore velocity is constant, $u_p = q/(\phi A)$, and Eq.(1) can be solved analytically by using the initial and boundary conditions

$$C(x \geq 0, t = 0) = C_i \qquad C(x = 0, t > 0) = C_0 \qquad C(x \to \infty, t \geq 0) = 0 \qquad (3)$$

And obtain

$$C^* = \frac{C - C_i}{C_0 - C_i} = \frac{1}{\sqrt{\pi}} \int_{\beta}^{\infty} \exp\left(-\kappa^2\right) d\kappa + \frac{1}{\sqrt{\pi}} \exp\left(\frac{x u_{p0}}{D_L}\right) \int_{a}^{\infty} \exp\left(-\kappa^2\right) d\kappa \quad (4)$$

where

$$\beta = \frac{x - u_{p0} t}{2(D_L t)^{1/2}} \qquad \alpha = \frac{x + u_{p0} t}{2(D_L t)^{1/2}} \quad (5)$$

If the perturbation of the local permeability (local heterogeneity) is strong enough, then the amplitude of the fluctuations of the mean pore velocity may vary over a broad range, and hence the assumption of homogeneous medium characterized by single values of longitudinal dispersion coefficient and mean pore velocity becomes questionable [9]. In an attempt to account for the effect of the strong fluctuations of the mean flow velocity on the longitudinal dispersion coefficient, solute dispersion is assumed to occur in a pore system consisting of two parallel regions, each characterized by individual values of mean pore velocity and longitudinal dispersion coefficient (Fig.2b). By ignoring transverse diffusion and any mass exchange between the two regions, Eqs.(4) and (5) can be applied separately to each region to compute the spatio-temporal evolution of the local concentration $C_j(u_{pj}, D_{Lj})$, $j = 1,2$. Then, the flux-averaged solute concentration at a cross-section can be calculated by the mass-balance

$$C^* = \frac{f u_{p1} C_1^* + (1-f) u_{p2} C_2^*}{f u_{p1} + (1-f) u_{p2}} \quad (6)$$

where f and $1-f$ are the fractions of the total cross-section area belonging to region 1 and 2, respectively, whereas the mean pore velocity, u_{p0}, is given by

$$u_{p0} = f u_{p1} + (1-f) u_{p2} \quad (7)$$

Moreover, in strongly heterogeneous porous media, the different time-scales of solute transport through pore networks of different permeability can be modelled by the 2-parameter multi-region model[6].

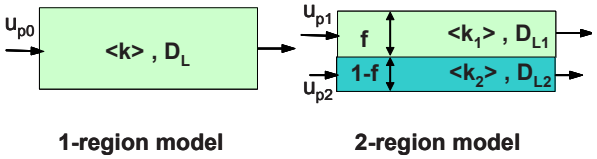

Fig. 2. Models used to simulate miscible displacement in homogeneous (1-region) and moderately heterogeneous (2-region) porous media.

2.3. Numerical modeling of immiscible displacement

The 1-dimensional immiscible displacement of water by oil (without source/sink terms) in a single-permeability porous medium (Fig.3a) is described by the following simplifying equations (Fig.3a)

$$\phi \frac{\partial S_i}{\partial t} + \frac{\partial u_i}{\partial x} = 0 \quad (8)$$

$$u_i = \frac{kk_{ri}}{\mu_i}\left(-\frac{\partial P_i}{\partial x} + \rho_i g\right) \tag{9}$$

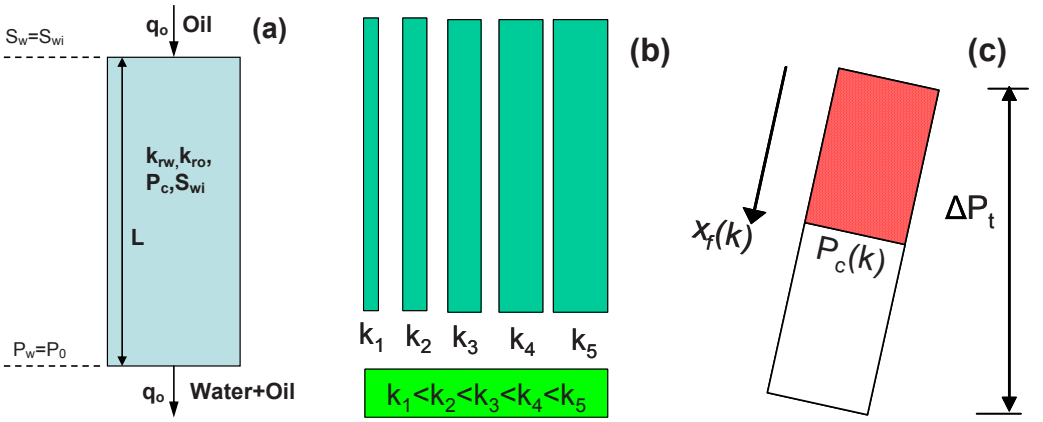

Fig. 3. (a) Single-permeability, and (b,c) multi-flow path models, used to simulate rate-controlled immiscible displacement in porous media.

Moreover, the capillary pressure is defined as the difference between the local pressures of the two fluids and is written as

$$P_c = P_o - P_w \tag{10}$$

whereas the fluid saturations are interrelated by

$$S_w + S_o = 1.0 \tag{11}$$

The piezometric pressure of each phase at distance x from the inlet is defined by the equation

$$P_i' = P_i - \rho_i g x \tag{12}$$

and the piezometric capillary pressure is written as

$$P_c' = P_c + (\rho_w - \rho_o) g x \tag{13}$$

Defining the oil fractional flow, F_o, as the ratio of the local oil velocity, u_{lo}, to the total superficial velocity, u_0 $(= q_o / A)$, namely

$$F_o = \frac{u_{lo}}{u_0} \qquad 0 \le F_o \le 1.0 \tag{14}$$

and using the dimensionless variables

$$\xi = \frac{x}{L} \quad \text{and} \quad \tau = \frac{u_0 t}{\phi L} \tag{15}$$

where L is the length of the porous medium, Eqs.(8)-(15) yield

$$\frac{\partial S_o}{\partial \tau} + \frac{\partial F_o}{\partial \xi} = 0 \tag{16}$$

$$F_o = \frac{k_{ro}}{\kappa k_{rw} + k_{ro}} \left(1 - \frac{u_c}{u_0} k_{rw} \frac{\partial P_c^{'*}}{\partial \xi} \right) \tag{17}$$

where, κ, is the viscosity ratio given by

$$\kappa = \frac{\mu_o}{\mu_w} \tag{18}$$

$P_c^{'*}$ is a dimensionless piezometric capillary pressure, defined by

$$P_c'^{*} = \frac{P_c'}{\Delta P_o^0}" = \frac{P_c}{\Delta P_o^0} + \frac{(\rho_w - \rho_o) g L \xi}{\Delta P_o^0} = P_c^* + \frac{(\rho_w - \rho_o) g L \xi}{\Delta P_o^0} \tag{19}$$

ΔP_o^0 is the experimentally measured pressure drop along the oil phase at steady-state ($t \to \infty$), and u_c is a characteristic superficial flow velocity defined by

$$u_c = \frac{k \Delta P_o^0}{\mu_w L} \tag{20}$$

The system of partial differential equations, Eqs.(16)-(17) is subject to the initial condition

$$S_o(0, \xi) = 0 \tag{21}$$

and boundary conditions

$$S_o(\tau, 0) = 1 - S_{wi} \tag{22}$$

$$S_o(\tau, 1) = 0 \tag{23}$$

where S_{wi} is the irreducible saturation of the wetting phase. Eq.(23) expresses the capillary end effect, arising from the sharp disappearance of the capillary pressure at the outlet of the porous medium [11,12].

For the analytical representation of capillary pressure and relative permeability curves, the following simplified Corey-type functions were selected

$$P_c = P_c^0 \left(1 - S_o^* + h_c \right)^{-m_c} \tag{24}$$

$$k_{rw} = k_{rw}^0 \left(1 - S_o^* + h_w \right)^{m_w} \Big/ \left(1 + h_w \right)^{m_w} \tag{25}$$

$$k_{ro} = k_{ro}^0 \left(S_o^* + h_o \right)^{m_o} \Big/ \left(1 + h_o \right)^{m_o} \tag{26}$$

where $S_o^* = S_o / (1 - S_{wi})$ is a dimensionless oil saturation.

For primary drainage, the water end relative permeability is $k_{rw}^0 = 1$, while for parameters h_w, h_o a constant value was selected ($h_w = h_o = 10^{-4}$). The set of parameters ($k_{ro}^0, m_w, m_o, P_c^0, m_c, h_c, S_{wi}$) are

estimated by fitting the measured to the calculated transient responses of the average soil segment saturations and total pressure drop at varying values of the capillary, Ca, defined by

$$Ca = \frac{q_o \mu_o}{A \gamma_{ow}} \tag{27}$$

where γ_{ow} is the oil/water interfacial tension.

The multi-flow path model (MFPM) can be used to quantify the heterogeneity of underground formations in larger scales and at the same time to determine the capillary pressure and relative permeability curves [8]. In very heterogeneous porous formations, the broad range of pore length scales may result in the creation of highly permeable (critical) pathways which transfer most of the flow and control the permeability and electrical conductivity of the soil [13]. Because of their high permeability, these flow pathways exhibit the smallest capillary resistance to the invasion of the non-wetting fluid and hence they also act as preferential flow paths during drainage. The pore space is regarded as a system of parallel flow paths (Fig.3b) which are characterized by a distribution of macro-scale permeability, $f\left(k^*;\sigma_{k^*}\right)$. The standard deviation, σ_{k^*}, is a measure of the soil macro-heterogeneity, as it indicates the degree of uniformity among the various flow paths. Each flow path can be regarded as a subset of the various pore systems (pore-and-throat networks) comprising the soil pore space, and its effective permeability results from averaging over this subset of pore systems. Differences between the subsets of pore systems specify the permeability distribution of the flow paths [14]. The mean length of the flow paths L_{fp} is defined by a common tortuosity factor, $\lambda = L/L_{fp}$, where L is the soil column length. The oil/water displacement in each flow path is assumed frontal and described by the irreducible wetting phase saturation, S_{wi}, and end oil relative permeability $k_{ro}^0 = k_{ro}\left(S_w = S_{wi}\right)$. In order to relate the capillary pressure of displacement with the effective permeability of each flow path, a 2-parameter Leverett type equation of the form

$$P_c(k) = \left(c\gamma_{ow}\cos\theta\right)k^{-\delta} \tag{28}$$

was used. Using mass and momentum balances, oil/water displacement was described by a system of integral & differential equations with dependent variables the dimensionless total pressure drop, $\Delta P_t^*(\tau)$ and positions, $\xi_f\left(k^*\right)$ of oil/water interfaces (fronts) along the flow paths (Fig.3c) [8]. Presuming that all abovementioned parameters of MFPM are known, then the transversely averaged oil saturation, S_o, calculated at the current axial positions of the interfaces (fronts), $\xi_f\left(k^*\right)$, is computed as a function of the corresponding capillary pressures P_c, Eq.(28), to estimate the capillary pressure curve, $P_c(S_o)$. Respectively, the oil and water relative permeability can be calculated as functions of the local oil saturation, S_o, or equivalently of the current positions of the fronts in flow paths, $\xi_f\left(k^*\right)$, by using the relationships

$$k_{ro}\left(\xi_f\right) = k_{ro}^0 \int_{k^*(\xi_f)}^{k^*_{max}} k^* f\left(k^*\right) dk^* \tag{29}$$

$$k_{rw}\left(\xi_f\right) = \int_{k^*_{min}}^{k^*(\xi_f)} k^* f\left(k^*\right) dk^* \tag{30}$$

3. Results and discussion

The estimation of the hydrodynamic dispersion and two-phase flow parameters was done with inverse modeling of experimental datasets in the environment of Athena Visual Studio software package [15]. For the homogeneous soil S1 the one-region (Fig.2) and single-permeability (Fig.3a) models were used. For the moderately heterogeneous soil S5, the one-region / two-region (Fig.2) and single-permeability / multi-flow path (Fig.3) models were used.

For S1 the longitudinal dispersivity, $a_L \approx 150-300\,\mu m$, is comparable to the mean grain size $\langle d_g \rangle \approx 200\,\mu m$ [9]. Both one-region and two-region models are capable of reproducing the solute concentration breakthrough curves of S5 (Fig.4), and the estimated pore velocity, u_{p0}, is comparable to its actual value, u_p (Table 2). For S5, the longitudinal dispersivity estimated by both models is one order of magnitude larger than that of S1 (Table 2). However, the 2-region model is more reliable, since it yields a more stable dispersivity and varying weakly with pore velocity, whereas the difference of estimated pore velocities, $u_{p1}-u_{p2}$, is a measure of soil heterogeneity as reflected in the transient response of the thickness of dispersion front [9].

Table 2. Hydrodynamic dispersion parameters for soil S5.

1-region model				2-region model					
u_p (m/s)	D_L/D_m	u_{p0} (m/s)	a_L (mm)	D_{L1}/D_m	D_{L2}/D_m	u_{p1}/u_{p2}	u_{p0} (m/s)	a_{L1} (mm)	a_{L2} (mm)
3.1×10^{-6}	15.8	3.1×10^{-6}	8.1	6.0	6.7	1.49	3.0×10^{-4}	3.9	2.9
5.8×10^{-6}	12.9	6.1×10^{-6}	3.4	9.7	14.6	1.46	6.1×10^{-4}	2.6	2.7
8.8×10^{-6}	32.3	9.3×10^{-6}	5.5	18.4	23.8	1.31	9.1×10^{-4}	3.6	3.6

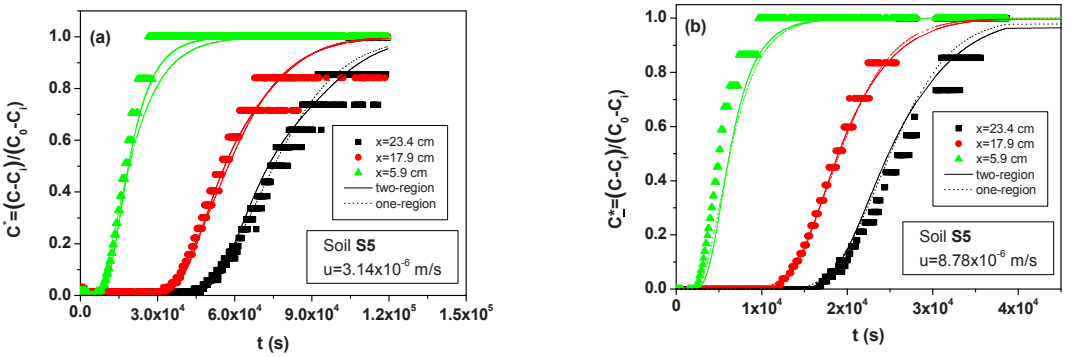

Fig. 4. Experimentally measured vs numerically predicted transient response of the solute concentration in soil column S5 for pore velocity (a) $u_p=3.1\times10^{-6}$ m/s, (b) $u_p=8.8\times10^{-6}$ m/s.

The capillary pressure and relative permeability curves estimated by the single-permeability model (Fig.3a) for both soils are shown in Figs. 5 and 6, respectively. The broad grain (and pore) size distribution of soil S5 is reflected in high oil relative permeability, k_{ro}, and low water relative permeability, k_{rw}, over low oil saturations, S_o (Fig.6b), whereas the capillary pressure of S5 shifts to higher values (Fig.5b).

The single-permeability model is unable to account for the preferential flow through (potentially) high permeability pathways, and estimate a broad capillary pressure curve commonly associated with a broad

pore-size distribution (Fig.7). A broad capillary pressure curve, analogous to that measured by Hg intrusion porosimetry was estimated by inverting the same dataset with the MFPM (Fig.8a). Respectively, the oil relative permeability curve increases rapidly at very low oil saturation values and asymptotically tends to unity for fast displacements (Fig.8b). This behaviour can be explained by considering the pore space as an interconnected cluster of pore networks dominated by different pore-throat sizes. During a drainage experiment oil will occupy the high hydraulic conductivity pore networks that comprise a small fraction of the total pore volume, and therefore oil breakthrough will take place at a relatively low capillary pressure while oil relative permeability will increase rapidly at very low oil saturation [14].

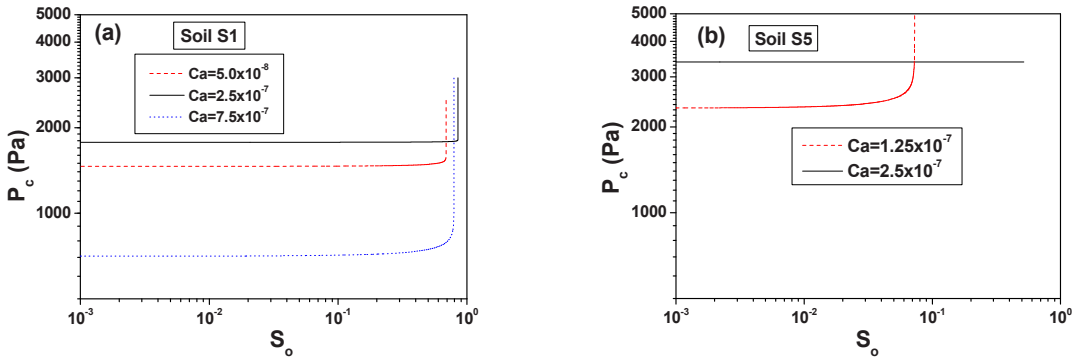

Fig. 5. Dynamic capillary pressure curves of soil estimated from rate-controlled n-C_{12}/water drainage experiments by using the single-permeability model: (a) soil S1; (b) soil S5.

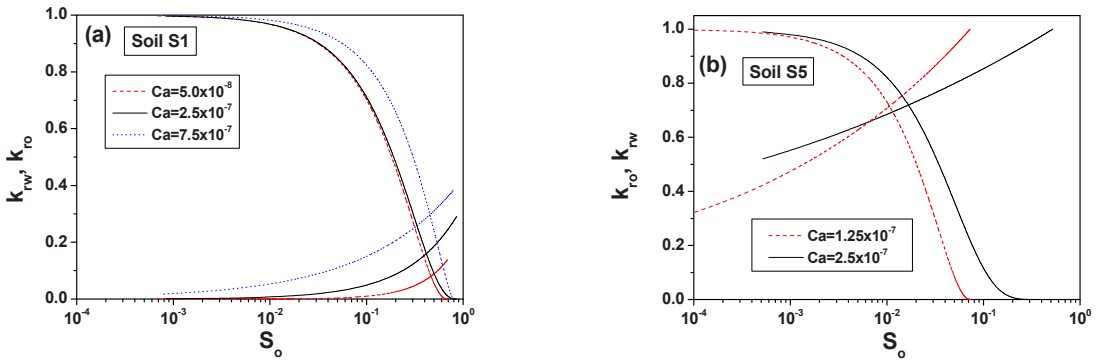

Fig. 6. Relative permeability curves of soil columns estimated from rate-controlled n-C_{12}/water drainage experiments by using the single-permeability model: (a) soil S1; (b) soil S5.

A plasma discharge technology has been used to remediate some layers (soil thickness~1-2 mm) of the aforementioned two soil types (S1, S5) pre-contaminated by a model non-aqueous phase liquid (NAPL) of n-C_{10}, n-C_{12}, n-C_{16} [16]. In general, NAPL blobs are expected to occupy pores from larger to smaller sizes. At low NAPL saturation, the air, flowing in parallel to the soil layer and above it, is accessible to NAPL blobs, and the "in-plane" NAPL oxidation in S1 is expected to proceed uniformly in accordance with the narrow pore size distribution and uniform sizes of NAPL blobs. In contrast, in S5, the smaller air/NAPL interfacial area of large NAPL-occupied pores may lead weaker "in-plane" NAPL oxidation rate and subsequently to lower NAPL removal efficiency. At high NAPL saturation, in both soils, the majority of the pore space is occupied by NAPL, except of very small pores, and initially the in-plane air/NAPL interfacial area, available for "in-plane" oxidation, is limited. Under such conditions, the

air overlying the soil favors the through-plane (vertical) NAPL oxidation which is expected to be slow and independent of soil heterogeneity.

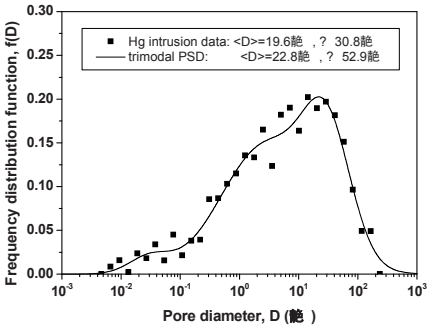

Fig. 7. Pore-throat diameter distribution of soil S5 obtained by differentiating the Hg intrusion curve. The experimental data were fitted with a tri-modal distribution function composed of three overlapping log-normal distributions.

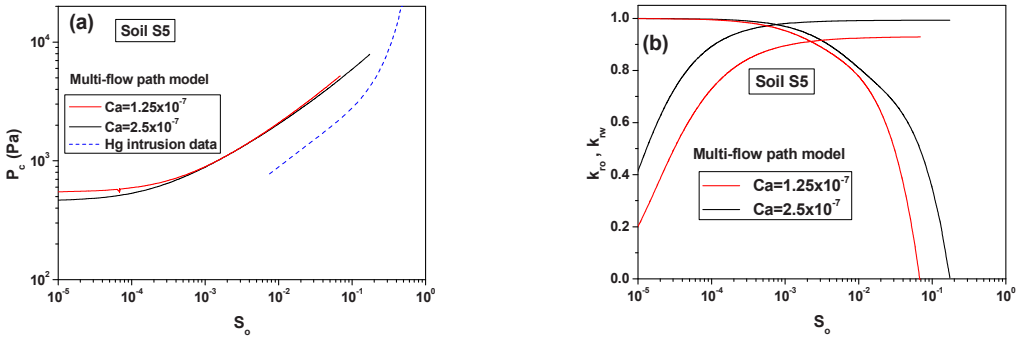

Fig. 8. (a) Capillary pressure, and (b) relative permeability curves of soil S5 estimated from rate-controlled n-C_{12}/water drainage experiments by using the MFPM.

4. Conclusions

A method was developed to quantify the multiphase transport properties along with the heterogeneity of soils by employing datasets of flow tests performed on soil columns, with adequate fluid transport models. The method is demonstrated with application to two soil types: (1) one homogeneous silicate sand, and (2) one moderately heterogeneous loamy sand. Miscible displacement tests conducted on soil columns are analyzed with the one-region and two-region models, whereas immiscible displacement tests are analyzed with the single-permeability and multi-flow path (MFPM) models. The two-region model provide information for the heterogeneity of the pore space at the pore network scale (micro-heterogeneity), and simultaneously enables us to estimate the dispersion coefficient. The MFPM quantifies soil heterogeneity at the soil column scale (macro-heterogeneity) and allows us to estimate explicitly the capillary pressure and relative permeability curves. The multiphase transport properties of soils are closely related with the pore structure properties and are correlated with the physical-chemical mechanisms of soil remediation technologies.

Acknowledgements

This research has been co-financed by the European Union (European Social Fund – ESF) and Greek National Funds through the Operational Program "Education and Lifelong Learning" of the National Strategic Reference Framework (NSRF) - Research Funding Program: Supporting Postdoctoral Researchers.

References

[1] Avraam DG, Payatakes AC. Flow regimes and relative permeabilities during steady-state two-phase flow in porous media. *J. Fluid Mech* 1995;**293**:207-36.
[2] Chen J, Hopmans JW, Grismer ME. Parameter estimation of two-fluid capillary pressure-saturation and permeability functions. *Adv. Water Resour* 1999;**22**:479-93.
[3] Tsakiroglou CD, Theodoropoulou M, Karoutsos V. Non-equilibrium capillary pressure and relative permeability curves of porous media. *AIChE J* 2003;**49:**2472-86.
[4] Tsakiroglou C.D, Theodoropoulou MA, Karoutsos V, Papanicolaou D. Determination of the effective transport coefficients of pore networks from transient immiscible and miscible displacement experiments. *Water Resources Research* 200;**41**(2):W02014.
[5] Inoue M, Simunek J, Shiozawa S, Hopmans JW. Simultaneous estimation of soil hydraulic and solute transport parameters from transient infiltration experiments. *Adv. Water Resour* 2000;**23**:677-88.
[6] Aggelopoulos CA, Tsakiroglou CD. Quantifying the Soil Heterogeneity from Solute Dispersion Experiments. *Geoderma* 2008;**146**:412-24.
[7] Aggelopoulos CA, and Tsakiroglou CD. The effect of micro-heterogeneity and capillary number on capillary pressure and relative permeability curves of soils. *Geoderma* 2008;**148**:25-34.
[8] Aggelopoulos CA, Tsakiroglou CD. A multi-flowpath model for the interpretation of immiscible displacement experiments in heterogeneous soil columns. *J. Contam. Hydrol* 2009;**105**:146-60.
[9] Aggelopoulos CA, Tsakiroglou CD. The longitudinal dispersion coefficient of soils as related to the variability of local permeability. *Water, Air and Soil Pollution* 2007;**185**:223-37.
[10] Aggelopoulos CA, Klepetsanis P, Theodoropoulou M, Pomoni K, Tsakiroglou CD. Large-scale effects on resisitivity index of porous media. *J. Contam. Hydrol* 2005;**77**:299-323.
[11] Huang DD, Honarpour MM. Capillary end effects in coreflood calculations. *J. Pet. Sci. Eng* 1998;**19**:103-17.
[12] Toth J, Bodi T, Szucs P, Civan F. Convenient formulae for determination of relative permeability from unsteady-state fluid displacements in core plugs. *J. Pet. Sci. Eng* 2002;**36**:33-44.
[13] Tsakiroglou CD, Ioannidis MA. Dual porosity modeling of the pore structure and transport properties of a contaminated soil. *Eur. J. Soil Sci* 2008;**59**:744-61.
[14] Tsakiroglou CD. A method to calculate the multiphase flow properties of heterogeneous porous media by using network simulations. *AIChE J* 2001;**57**:2618-28.
[15] Stewart WE, Caracotsios M, Sorensen JP. Parameter estimation from multiresponse data. *AICHE J* 1992;**38**:641-50.
Aggelopoulos CA, Tsakiroglou CD, Ognier S, Cavadias S. Ex situ soil remediation by cold atmospheric plasma discharge. *Procedia Env. Sci* 2013.